

Contextual Gesture: Co-Speech Gesture Video Generation through Context-aware Gesture Representation

Pinxin Liu¹ Pengfei Zhang² Hyeonwoo Kim³ Pablo Garrido⁴ Ari Sharpio⁴ Kyle Olszewski⁴

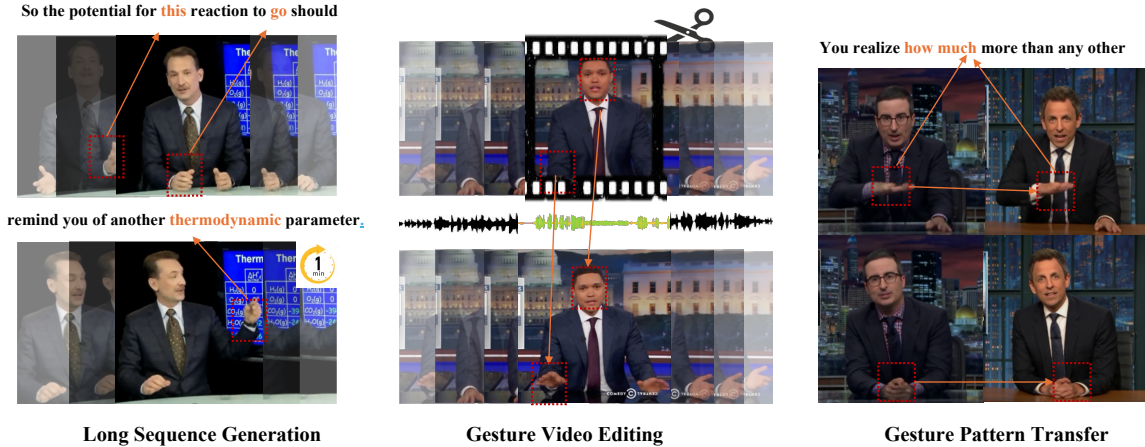


Figure 1: Contextual Gesture achieves various fine-grained control over video-level gesture motion. **Left:** We can generate 30s to 1 min speech conditioned gesture videos. **Mid:** We modify the gestures for intermediate frames of a video by providing a new audio segment. **Right:** Different people present the same gesture patterns for a given audio.

Abstract

Co-speech gesture generation is crucial for creating lifelike avatars and enhancing human-computer interactions by synchronizing gestures with speech. Despite recent advancements, existing methods struggle with accurately identifying the rhythmic or semantic triggers from audio for generating contextualized gesture patterns and achieving pixel-level realism. To address these challenges, we introduce Contextual Gesture, a framework that improves co-speech gesture video generation through three innovative components: (1) a chronological speech-gesture alignment that temporally connects two modalities, (2) a contextualized gesture tokenization that incorporate speech context into motion pattern representation through distillation, and (3) a structure-aware refinement module that employs edge connection to link gesture keypoints to improve video generation. Our extensive experiments

demonstrate that Contextual Gesture not only produces realistic and speech-aligned gesture videos but also supports long-sequence generation and video gesture editing applications, shown in Fig. 1 Project Page: <https://andypinxinliu.github.io/Contextual-Gesture/>.

1. Introduction

In human communication, speech is often accompanied by gestures that enhance understanding and convey emotions (De Ruiter et al., 2012). As these non-verbal cues play a vital role in effective interaction (Burgoon et al., 1990), gesture generation plays a key component of natural human-computer interactions: equipping virtual avatars with realistic gesture capabilities become essential in creating immersive interactive experiences.

The relationships between the semantic and emotion content of speech context, the corresponding gestures, and the visual appearance of the speaker’s performance are complex. As such, many recent works (Yi et al., 2023; Liu et al., 2023; 2022d;a) address a reduced form of this problem by generating a simplified representation of the 3D motion, consisting of joints and body parts, that plausibly accompanies a given speech sample, which can then be rendered using standard rendering pipelines. Such representations capture basic

¹University of Rochester, USA ²University of California Irvine, USA ³Imperial College, London, UK ⁴Flaswless AI, USA. Correspondence to: Kyle Olszewski <kyle.olszewski@flawlessai.com>.

motion patterns, yet they neglect the importance of the speaker’s visual appearance, resulting in a lack of realism that hinders effective communication.

Other works, *e.g.* ANGIE (Liu et al., 2022c) and S2G-diffusion (He et al., 2024), employ image-warping techniques, constrained by keypoints obtained from optical-flow-based deformations, for co-speech video generation. However, such approaches encounter several critical issues. First, these keypoints only define large-scale transformations, and thus miss subtle movements of specific body parts (*e.g.* hands, fingers). Second, this broad and unconstrained motions representation neglects the triggers associated with gestures, specifically the contextual information from speech. This approach fails to provide the generator with the intrinsic connections between speech context and gesture motion, making it challenging for the generator to produce motion patterns that effectively convey the speaker’s metaphorical expressions or intentions. Finally, the generated motion patterns are often unstructured and overly reactive to large motion, resulting in noisy and imprecise renderings, especially in the hands and shoulders. Collectively, these challenges significantly limit the overall quality and realism of the generated video content.

To address these challenges, we introduce *Contextual Gesture*, a framework designed to generate speech-aligned gesture motions and high-fidelity speech video outputs. Our approach begins with gesture motion representations using keypoints from human pose estimators. To uncover the intrinsic temporal connections between gestures and speech, we employ chronological contrastive learning to align these two modalities. This joint representation captures the triggers of gesture patterns influenced by speech. We incorporate speech-contextual features into the tokenization process of gesture motions through knowledge distillation, aiming to infuse the gesture representations with implicit intentions conveyed in the audio. This integration creates a clear linkage between the gestures and the corresponding speech, enabling the generation of gestures that reflect the speaker’s intended meaning. For motion generation, we leverage a masking-based gesture generator that refines the alignment of gesture motions with the speech signal through bidirectional mask pretraining. Finally, for uplifting the latent motion generation into 2D animations, we propose a structure-aware image refinement module that generates heatmaps of edge connections from keypoints, providing image-level supervision to improve the quality of body regions with large motion. Extensive experiments demonstrate that our method outperforms the existing approaches in both quantitative and qualitative metrics and achieves long sequence generation and editing applications.

In summary, our primary contributions are:

1. *Contextual Gesture*, a framework that achieves joint contextualized gesture motion and video generation with various application support;
2. a *Context-aware gesture representation* obtained through knowledge distillation from the chronological gesture-speech aligned features from chronological contrastive learning; and
3. a *Structural-aware Image refinement module*, with edge heatmaps as supervision to improve video fidelity.

2. Related Work

Co-speech Gesture generation Most recent works on co-speech gesture generation employ skeleton- or joint-level pose representations. (Ginosar et al., 2019) use an adversarial framework to predict hand and arm poses from audio, and leverage conditional generation (Chan et al., 2019) based on pix2pixHD (Wang et al., 2018) for videos. Some recent works (Liu et al., 2022d; Deichler et al., 2023; Xu et al., 2023; Ao et al., 2022) learn the hierarchical semantics or leverage contrastive learning to obtain joint audio-gesture embedding from linguistic theory to assist the gesture pose generation. TalkShow (Yi et al., 2023) estimates SMPL (Pavlakos et al., 2019) poses, and models the body and hand motions for talk-shows. CaMN (Liu et al., 2022b), EMAGE (Liu et al., 2023) and Diffshg (Chen et al., 2024) use large conversational and speech datasets for joint face and body modeling with diverse style control. ANGIE (Liu et al., 2022c) and S2G-Diffusion (He et al., 2024) use image-warping features based on MRAA (Siarohin et al., 2021) or TPS (Zhao & Zhang, 2022) to model body motion and achieve speech driven animation by learning correspondence between audio and image-warping features. However, none of these works produce structure- and speech-aware motion patterns suitable for achieving natural and realistic gesture rendering.

Conditional Video Generation Conditional Video Generation has undergone significant progress for various modalities, like text (Blattmann et al., 2023), pose (Karras et al., 2023; Wang et al., 2023), and audio (Ruan et al., 2023). AnimateDiff (Guo et al., 2024b) presents an efficient low-rank adaptation (Hu et al., 2022) (LoRA) to adapt image diffusion model for video motion generation. AnimateAnyone (Hu et al., 2023) construct referencenet for fine-grained control based on skeleton. Make-Your-Anchor (Huang et al., 2024) and Champ (Zhu et al., 2024) improve avatar video generation through face and body based on SMPL-X conditions. EMO (Tian et al., 2024) and EchoMimic (Meng et al., 2024) leverages audio as control signal for talking head and upper body generation. However, these methods are slow in inference speed and ignore the gesture patterns or rhythmic or semantic signals from audio.

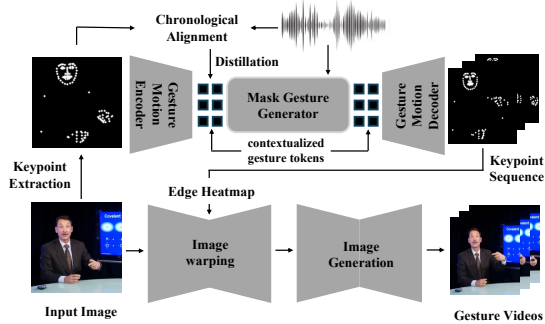


Figure 2: An overview of our framework. We extract keypoints and leverage chronological alignment with distillation to achieve contextualized gesture motion representation. We leverage a masking-based generator conditioned on audio to generate gesture keypoint sequences and apply image warping with refinement based on edge heatmaps for final gesture video generation.

3. Contextual Gesture

Shown in Fig. 2, our framework targets at generating co-speech photo-realistic human videos with contextualized gesture patterns. To achieve this goal, we first learn contextual-aware gesture motion representation through knowledge distillation based on chronological gesture-speech alignment (Sec. 3.1). We leverage a Masking-based Gesture Generator for gesture motion generation. (Sec. 3.2) To improve the noisy hand and shoulder movement during the transfer of latent motion to pixel space, we propose a structure-aware image refinement through edge heatmaps for guidance. (Sec. 3.3).

3.1. Contextualized Gesture Representation

Generating natural and expressive gestures requires capturing fine-grained contextual details that conventional approaches often overlook. Consider a speaker emphasizing the word “really” in the sentence “I really mean it” - while existing methods might generate a generic emphatic gesture, they typically fail to capture the subtle, context-specific body movements that make human gestures truly expressive. This limitation stems from relying solely on motion quantization, which often loses the nuanced relationship between speech and corresponding gestures.

To address this challenge, we propose a novel approach that integrates both audio and semantic information into the motion quantizer’s codebook. This integration requires solving two fundamental problems. First, we need to understand how gestures align with speech not just at a high level, but in terms of precise temporal correspondence - when specific words or phrases trigger particular movements, and how the rhythm of speech influences gesture timing. To capture these temporal dynamics, we develop a chronological gesture-speech alignment framework using

specialized contrastive learning. Second, we leverage knowledge distillation to incorporate this learned temporal alignment information into the gesture quantizer, enabling our system to generate gestures that are synchronized with speech both semantically and rhythmically.

Feature Representation. We utilize 2D poses extracted from images to formulate gestures by facial and body movements. We represent a gesture motion sequence as $G = [F; B] = [f_t; b_t]_{t=1}^T$, where T denotes the length of the motion, f represents the 2D facial landmarks, and b denotes the 2D body landmarks. For speech representation, we extract audio embeddings from WavLM (Chen et al., 2022) and Mel spectrogram features (Rabiner & Schafer, 2010) and beat information using librosa (McFee et al., 2015). For text-semantics, we extract embedding from RoBERTa (Liu et al., 2019). These features are concatenated to form the speech representation.

Chronological Speech-Gesture Alignment. Traditional approaches to modality alignment (Ao et al., 2022; Liu et al., 2022d; Deichler et al., 2023) rely on global representations through class tokens or max pooling, which overlook the fine-grained temporal dynamics between speech and gestures. We address this limitation by introducing chronological modality alignment.

Vanilla Contrastive Alignment. To align gesture motion patterns with the content of speech and beats, we first project both speech and gesture modalities into a shared embedding space to enhance the speech content awareness of gesture features. As illustrated in Fig. 3 Middle, we separately train two gesture content encoders, \mathcal{E}_f for face motion and \mathcal{E}_b for body motion, alongside two speech encoders, \mathcal{E}_{S_f} and \mathcal{E}_{S_b} , to map face and body movements and speech signals into this joint embedding space. For simplicity, we represent the general gesture motion sequence as G . We then apply mean pooling to aggregate content-relevant information to optimize the following loss (van den Oord et al., 2019):

$$\mathcal{L}_{\text{NCE}} = -\frac{1}{2N} \sum_i \left(\log \frac{\exp S_{ii}/\tau}{\sum_j \exp S_{ij}/\tau} + \log \frac{\exp S_{ii}/\tau}{\sum_j \exp S_{ji}/\tau} \right), \quad (1)$$

where S computes the cosine similarities for all pairs in the batch, defined as $S_{ij} = \cos(z_i^s, z_j^g)$ and τ is the temperature.

Chronological Negative Examples. While vanilla Contrastive Learning builds global semantical alignment, we further propose to address the temporal correspondence between speech and gesture. As shown in Fig. 3 Left, consider a speaker saying, “After watching that video, you realize how much, more than any other president...”. In this case, the gesture sequence involves “knocking at the table” when saying “more than any other,” serving as a visual emphasis for “how much” to highlight the point. To encourage the model understand both semantic and rhythmic alignment between two modalities, we shuffle

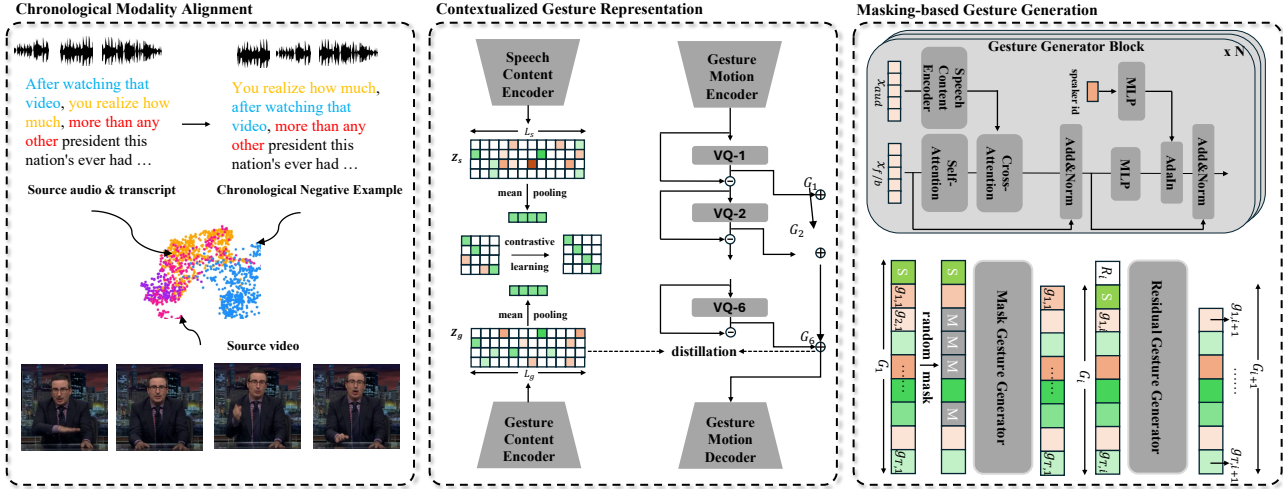


Figure 3: **Left:** Chronological Contrastive Learning for gesture-speech alignment. **Mid:** We distill the contextual-aware feature into latent codebook. **Right:** Gesture motion generation based on Mask and Residual Gesture Generator.

the words and their corresponding phonemes. By shuffling the sequence to "you realize how much, after watching that video," the semantic intention of the speech is preserved, but the rhythmic correspondence between speech and gesture is disrupted. We use Whisper-X (Bain et al., 2023) to detect temporal segments in the raw sequences. We cut the audio and shuffle these segments, creating these augmented samples as additional chronological negative examples within a batch during contrastive learning.

Gesture Quantization with Distillation. To construct context-aware motion representations, we encode alignment information into the gesture motion codebook. This allows the semantics and contextual triggers from speech to be directly fused into the motion embedding, and enables the generator to easily identify the corresponding motion representation in response to speech triggers. To achieve this goal, we leverage gesture content encoder as the teacher and distill knowledge to codebook latent representation, shown in Fig. 3 Middle. We maximize the cosine similarity over time between the RVQ quantization output and the representation from the gesture content encoder:

$$\mathcal{L}_{\text{distill}} = \sum_{t=1}^T \cos(p(Q_R)^t, E_S(G)^t) \quad (2)$$

where p denotes a linear projection layer, Q_R is the final quantized output from the RVQ-VAE, $E_S(G)$ represents the output from the gesture content encoder, and T is the total time frames. The overall training objective is defined as:

$$\mathcal{L}_{\text{rvq}} = \|x - \hat{x}\|^2 + \alpha \sum_{r=1}^R \|e_r - \text{sg}(z_r - e_r)\|^2 + \beta \mathcal{L}_{\text{distill}} \quad (3)$$

where \mathcal{L}_{rvq} combines a motion reconstruction loss, a commitment loss (van den Oord et al., 2018) for each layer of quantizer with a distillation loss, with α and β weighting the contributions.

3.2. Speech-conditioned Gesture Motion Generation

For Motion Generator, we adopt a similar masking-based generation procedure as in MoMask (Guo et al., 2024a) due to its flexibility of editing and fast inference speed. We only include the generator data flows in the main paper but defer the training and inference strategy in the Appendix.

Mask Gesture Generator. As shown in Fig. 3 Right, during training, we derive motion tokens by processing raw gesture sequences through both body and face tokenizers. The motion token corresponding to the source image acts as the conditioning for all subsequent frames. For speech control, we initialize the audio content encoder from alignment pre-training as described in Sec. 3.1. This pre-alignment of gesture tokens with audio encoder features enhances the coherence of gesture generation. We employ cross-attention to integrate audio information and apply Adaptive Instance Normalization (AdaIN) (Huang & Belongie, 2017), enabling gesture styles based on the speaker’s identity.

Residual Gesture Generator. The Residual Gesture Generator shares a similar architecture with the Masked Gesture Generator, but it includes R separate embedding layers corresponding to each RVQ residual layer. This module iteratively predicts the residual tokens from the base layers, ultimately producing the final quantized output. Please see MoMask (Guo et al., 2024a) for further details.

3.3. Structure-Aware Image Generation

Converting generated gesture motions into realistic videos presents significant challenges, particularly in handling camera movement commonly found in talkshow and speech videos. While recent 2D skeleton-based animation methods (Hu et al., 2023) offer a potential solution, our empirical analysis (detailed in the Appendix) reveals that these approaches struggle with background stability in the presence of camera motion.

To address this limitation, we draw inspiration from optical-flow based image warping methods (Zhao & Zhang, 2022; Siarohin et al., 2021; 2019), which have shown promise in handling deformable motion. We adapt these approaches by replacing their unsupervised keypoints with our generated gesture keypoints from Sec. 3.2 for more precise foreground optical flow estimation. However, this estimation still presents uncertainties, resulting in blurry artifacts around hands and shoulders, particularly when speakers make rapid or large movements.

To address the uncertainties by optical-flow-based deformation during this process, we propose a Structure-Aware Generator. Auto-Link (He et al., 2023) demonstrates that the learning of keypoint connections for image reconstruction aids the model in understanding image semantics. Based on this, we leverage keypoint connections as semantic guidance for image generation.

Edge Heatmaps. Using the gesture motion keypoints, we establish linkages between them to provide structural information. To optimize computational efficiency, we limit the number of keypoint connections to those defined by body joint relationships (Wan et al., 2017), rather than all potential connections in (He et al., 2023).

For two keypoints \mathbf{k}_i and \mathbf{k}_j within connection groups, we create a differentiable edge map \mathcal{S}_{ij} , modeled as a Gaussian function extending along the line connecting the keypoints. The edge map \mathcal{S}_{ij} for keypoints $(\mathbf{k}_i, \mathbf{k}_j)$ is defined as:

$$\mathcal{S}_{ij}(\mathbf{p}) = \exp(v_{ij}(\mathbf{p})d_{ij}^2(\mathbf{p})/\sigma^2), \quad (4)$$

where σ is a learnable parameter controlling the edge thickness, and $d_{ij}(\mathbf{p})$ is the L_2 distance between the pixel \mathbf{p} and the edge defined by keypoints \mathbf{k}_i and \mathbf{k}_j :

$$d_{ij}(\mathbf{p}) = \begin{cases} \|\mathbf{p} - \mathbf{k}_i\|_2 & \text{if } t \leq 0, \\ \|\mathbf{p} - ((1-t)\mathbf{k}_i + t\mathbf{k}_j)\|_2 & \text{if } 0 < t < 1, \\ \|\mathbf{p} - \mathbf{k}_j\|_2 & \text{if } t \geq 1, \end{cases} \quad (5)$$

$$\text{where } t = \frac{(\mathbf{p} - \mathbf{k}_i) \cdot (\mathbf{k}_j - \mathbf{k}_i)}{\|\mathbf{k}_i - \mathbf{k}_j\|_2^2}. \quad (6)$$

Here, t denotes the normalized distance between \mathbf{k}_i and the projection of \mathbf{p} onto the edge.

To derive the edge map $\mathcal{S} \in \mathbb{R}^{H \times W}$, we take the maximum value at each pixel across all heatmaps:

$$\mathcal{S}(\mathbf{p}) = \max_{ij} \mathcal{S}_{ij}(\mathbf{p}). \quad (7)$$

Structural-guided Image Refinement. Traditional optical-flow-based warping methods are effective for handling global deformations but often fail under large motion patterns, such as those involving hands or shoulders, resulting in significant distortions. To address this, we

introduce a structure-guided refinement process that incorporates semantic guidance via structural heatmaps.

Instead of directly rendering the warped feature maps into RGB images, we first predict a low-resolution feature map of size $256 \times 256 \times 32$. Multi-resolution edge heatmaps are generated and used as structural cues to refine the feature maps. After performing deformation and occlusion prediction at each scale using TPS (Zhao & Zhang, 2022), the edge heatmaps are fed into the generator. Specifically, we integrate these heatmaps into the fusion block using SPADE (Park et al., 2019), enabling the precise prediction of residuals. These residuals are element-wise added to the warped feature maps, ensuring precise structural alignment.

To generate high-resolution RGB images, we employ a U-Net architecture that takes both the warped features and edge heatmaps as inputs. This design preserves fine-grained structural details while compensating for motion-induced distortions. Additional architectural details and analysis are provided in the Appendix.

Training Objective. We employ an adversarial loss, along with perceptual similarity loss (LPIPS) (Johnson et al., 2016) and pixel-level L_1 loss for image refinement. The reconstruction objective is defined as:

$$I_{\text{rec}} = \gamma \mathcal{L}_{GAN} + \mathcal{L}_{L1} + \mathcal{L}_{LPIPS}, \quad (8)$$

where I_{gt} denotes the ground-truth image, and I_{gan} represents the generated image. We leverage a small weighted term of γ to prevent GAN training collapse.

4. Experiments

Since our work focuses on joint gesture motion and video generation, the main experiments primarily compare our approach with existing methods that also address joint generation. Comparisons for gesture motion generation and avatar video rendering are deferred to the Appendix.

4.1. Experimental Settings

Dataset and Preprocessing. We utilize PATS (Ginosar et al., 2019; Ahuja et al., 2020) for the experiments. It contains 84,000 clips from 25 speakers with a mean length of 10.7s, 251 hours in total. For a fair comparison, following the literature (Liu et al., 2022c; He et al., 2024) and replace the missing subject, with 4 speakers are selected (*Noah*, *Kubinec*, *Oliver*, and *Seth*). All video clips are cropped with square bounding boxes, centering speaks, resized to 256×256 . We defer the additional details in the Appendix.

4.2. Gesture Video Generation

Evaluation Metrics. For gesture motion metrics, we use **Fréchet Gesture Distance (FGD)** (Yoon et al., 2020) to measure the distribution gap between real and generated gestures in feature space, **Diversity (Div.)** (Lee et al., 2019)



Figure 4: **Visual comparisons.** Our method generates high-quality hand and shoulder motions, and presents metaphoric gestures when saying “90 joules,” and “in each case.”. Red boxes denote the blurry or unnatural gestures by other methods.

to calculate the average feature distance between generated gestures, **Beat Alignment Score (BAS)** following (Li et al., 2021), and **Percent of Correct Motion parameters (PCM)**, difference of generation deviate from ground-truth following (Chen et al., 2024). We extract 2D human poses for face and body using MMPose (OpenMMLab, 2020). Note that in comparison with other models, the FGD is measured by the keypoints extracted from generated videos while in ablation studies, to prevent the effect image warping errors, FGD is measured by keypoints generated in Sec.3.2.

For pixel-level video quality, we assess **Fréchet Video Distance (FVD)** (Unterthiner et al., 2018) for the overall quality of gesture videos, **VQA_A** for aesthetics and **VQA_T** for technical quality based on Dover (Wu et al., 2023), pretrained on datasets with labels ranked by real users.

We further evaluate the training and inference efficiency of

various methods, **Train-T** denotes the number of days for training. **Infer-T** denotes the number of seconds to produce a 10-second video.

Baseline Methods. We benchmark Contextual Gesture against several co-speech gesture video generation methods: (1) ANGIE (Liu et al., 2022c), (2) S2G-Diffusion (He et al., 2024), (3) MM-Diffusion (Ruan et al., 2023), and (4) EchoMimicV2 (Meng et al., 2024). The first two are conventional optical-flow-based methods. MM-Diffusion is capable of achieving joint audio-visual generation. EchoMimicV2 is the most recent diffusion based speech-avator animation model pretrained on large scale data.

Evaluation Results. We present quantitative evaluations in Tab. 1. Our approach significantly outperforms existing methods in both gesture motion and video quality metrics. We provide qualitative evaluations in Fig. 4. MM-Diffusion

Table 1: Quantitative results shows our method performs better in terms of gesture motions and video generation quality.

Name	Gesture Motion Evaluation				Video Quality Assessment			Speed	
	FGD ↓	Div. ↑	BAS ↑	PCM ↑↑	FVD ↓	VQA _A ↑	VQA _T ↑	Train-T ↓	Infer-T ↓
Ground Truth	0.0	14.01	1.00	1.00	0.00	95.69	5.33	-	-
MM-Diffusion	67.56	4.32	0.65	0.11	-	77.65	4.14	14 days	600 sec
ANGIE	34.13	7.87	0.78	0.37	515.43	86.32	4.98	5 days	30 sec
S2G-Diffusion	10.54	10.08	0.98	0.45	493.43	94.54	5.63	5 days	35 sec
EchoMimicV2	13.65	9.85	0.98	0.45	466.84	95.65	5.98	-	1200 sec
Ours + AnimateAnyone	6.56	13.06	0.99	0.54	477.82	95.63	6.04	8.5 days	50 sec
Ours	8.76	13.13	0.99	0.54	466.43	96.53	6.12	6 days	3 sec

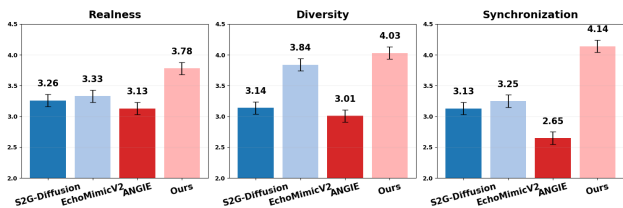


Figure 5: **User Study.** We generate 80 videos per method for evaluations of *Realness*, *Diversity*, and *Synchronization*.

is not able to handle complex motion patterns, leading to almost static results. ANGIE and S2G-Diffusion struggle with local regions, such as the hands, due to its reliance on unsupervised keypoints for global transformations, which neglects local deformations. EchoMimicV2 lacks the background motion modeling and is only capable of presenting the aligned centered avatars in the middle. In addition, it fails to achieve diversified gestures. In contrast, our method demonstrates high-quality video generation, particularly in the facial and body areas. The alignment between gesture and speech is notably enhanced through our speech-content-aware gesture latent representation. For example, when the actor says "90 joules," he points to the screen, and he emphasizes phrases like "so two ways" and "in each case" by raising his hands.

User Study. We conducted a user study to evaluate the visual quality of our method. We sampled 80 videos from each method including EchoMimicV2, S2G-Diffusion, ANGIE and ours and invited 20 participants to conduct Mean Opinion Scores (MOS) evaluations. The rating ranges from 1 (poorest) to 5 (highest). Participants rated the videos on: (1) MOS₁: "How *realistic* does the video appear?", (2) MOS₂: "How *diverse* does the gesture pattern present?", (3) MOS₃: "Are speech and gesture *synchronized* in this video?". The videos were presented in random order to capture participants' initial impressions. As shown in Fig. 5, our method outperformed others across realness, synchronization and diversity, achieving significant performance improvement over existing methods.

Table 2: **Ablation Studies** for keypoint design, gesture representation, generator architecture and image-refinement.

Kp Repr.	FVD ↓ LPIPS ↓ PSNR ↑			G-Repr. FGD ↓ PCM ↑	
	Unsup-kp	387.05	0.05	27.41	baseline
2D-pose	272.18	0.05	27.26	+RVQ	3.43 0.37
+ flex kp	377.14	0.06	25.36	+ distill	2.75 0.58
full	225.77	0.04	27.17	+ chrono	0.87 0.59

(a) Configs for keypoint design. (b) Gesture Repr.

G-Gen.	FGD ↓	PCM ↑	Refine	VQA _A ↑	VQA _T ↑	FVD ↓
w/o res	1.62	0.51	w/o refine	92.15	5.43	494.35
concat	3.55	0.51	+ UNet	93.86	5.51	478.54
w/o align	1.33	0.53	+ skeleton	95.79	5.65	473.34
full-model	0.87	0.59	+ heatmap	96.53	6.12	466.43

(c) Model Design. (d) Image-refinement strategies.

4.3. Ablation Study

We present ablation studies of keypoint design for image warping, gesture motion representation, generator architecture design, and various comparisons of image-refinement. We defer additional experiments in the Appendix.

Motion Keypoint Design. We evaluate four settings for image-warping: (1) unsupervised keypoints for global optical-flow transformation (as in ANGIE and S2G-Diffusion), (2) 2D human poses, (3) 2D human poses augmented with flexible learnable points, and (4) full-model reconstruction with refinement. Each design is assessed using TPS (Zhao & Zhang, 2022) transformation, with self-reconstruction based on these keypoints for evaluation. As shown in Tab. 2a, learnable keypoints lead to a significant decrease in FVD, highlighting their inadequacy for motion control. The inclusion of flexible keypoints does not enhance the image-warping outcomes. Consequently, we opt to utilize 2D pose landmarks exclusively for our study.

Motion Representation. We evaluate several configurations: (1) baseline: no motion representation, relying solely on the generator to synthesize raw 2D landmarks; (2) + RVQ: utilizing Residual VQ (RVQ) to encode joint face-body keypoints; (3) + distill: learning joint embeddings for speech and gesture in both face and body motions; (4) +

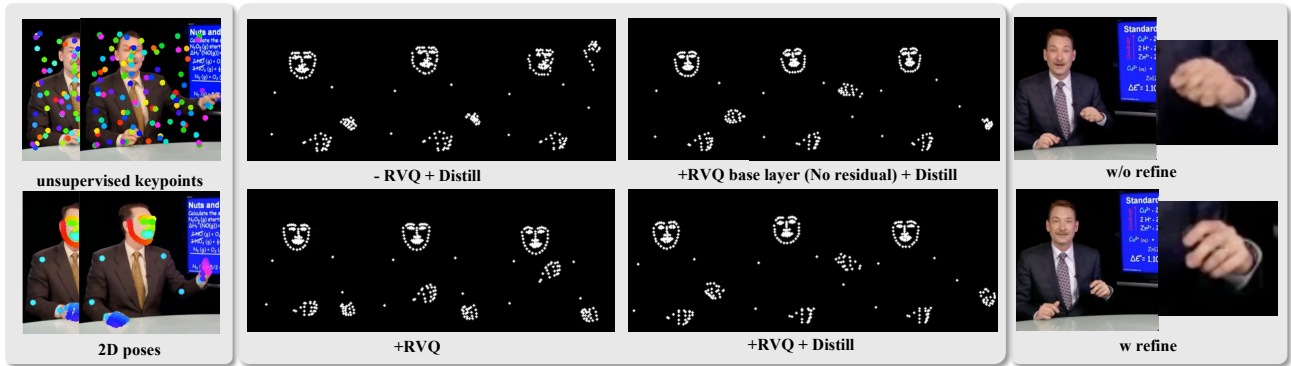


Figure 6: **Ablations.** Left: motion by unsupervised keypoints or 2d poses; Middle: RVQ-based gesture representation and generation; Right: image-refinement helps hand generation.

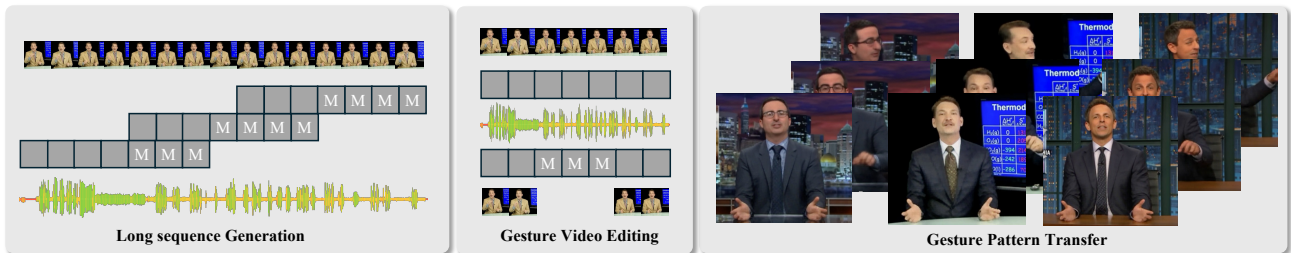


Figure 7: Our model supports multiple video gesture generation and editing applications.

chrono: leverage chronological alignment for distillation. We discover RVQ significantly improve the precise pose location while distillation leads to natural movements.

Generator Design. We explore various designs for the gesture generator: (1) w/o res: no residual gesture decoder; (2) concat: instead of using cross-attention for audio control, we concatenate the audio features with gesture latent features element-wise during generation; (3) w/o align: the audio encoder is randomly initialized rather than initialized from face and body contrastive learning. Our findings indicate that the Residual Gesture Generator significantly enhances finger motion generation. The cross-attention design outperforms element-wise concatenation, while the pre-alignment of the audio encoder notably improves FGD.

Image Refinement. We examine various network designs for motion generation, specifically: (1) w/o refine: no image refinement, relying solely on image warping; (2) + UNet: employing a standard UNet; (3) + pose skeleton: integrating connected skeleton maps as in the diffusion ReferenceNet (Hu et al., 2023); (4) + edge heatmap: substituting the previous design with our learnable edge heatmap. Our experiments reveal that the edge heatmap outperforms skeleton maps, due to the learnable thickness of connections for better semantic guidance.

4.4. Application

Long Sequence Generation. As in Fig. 7, to generate long sequences, we begin with the initial frame and corresponding target audio, segmented into smaller windows.

After generating the first segment, the last few frames of the output serve as the new starting condition for the next segment, enabling iterative outpainting.

Video Gesture Editing. For editing, we extract keypoints from the video, tokenize face and body movements into motion tokens, and insert mask tokens where edits are needed. By changing the speech audio or speaker identity, we can create new gesture patterns and re-render the video.

Gesture Pattern Transfer. With different identity embeddings, we generate unique gesture patterns for the same audio input. See the demo videos in the Appendix.

Speech-Gesture Retrieval. With chronological speech-gesture alignment, the model is capable of retrieving the best gesture motion corresponding to the given speech audio in a batch of data. See additional details in the Appendix.

5. Conclusion

We present **Contextual Gesture**, a framework for generating realistic co-speech gesture videos. To ensure the gestures cohere well with speech, we propose speech-content aware gesture motion representation through knowledge distillation from the gesture-speech aligned features. Our structural-aware image generation module improves the transformation of latent motions into realistic animations for large-scale body motions. We hope this work encourage further exploration of the relationship between gesture patterns and speech context for more compelling gesture video generations in the future.

6. Impact Statements

This work focuses on generating co-speech gesture videos, highlighting both its potential and ethical concerns, particularly the risk of misuse for creating deepfakes or fabricated events involving public figures. While it's impossible to fully eliminate such risks, the research provides a technical analysis of gesture video synthesis, emphasizing its capabilities and limitations. To mitigate misuse, we recommend practices like watermarking videos and using detection tools for synthetic content to promote responsible and ethical use of the technology.

References

- Ahuja, C., Lee, D. W., Ishii, R., and Morency, L.-P. No Gestures Left Behind: Learning Relationships between Spoken Language and Freeform Gestures. In *Proceedings of the 2020 Conference on Empirical Methods in Natural Language Processing: Findings*, pp. 1884–1895, 2020.
- Ao, T., Gao, Q., Lou, Y., Chen, B., and Liu, L. Rhythmic gesticulator: Rhythm-aware co-speech gesture synthesis with hierarchical neural embeddings. *ACM Transactions on Graphics (TOG)*, 41(6):1–19, 2022.
- Bain, M., Huh, J., Han, T., and Zisserman, A. Whisperx: Time-accurate speech transcription of long-form audio. *INTERSPEECH 2023*, 2023.
- Blattmann, A., Dockhorn, T., Kulal, S., Mendelevitch, D., Kilian, M., Lorenz, D., Levi, Y., English, Z., Voleti, V., Letts, A., Jampani, V., and Rombach, R. Stable Video Diffusion: Scaling Latent Video Diffusion Models to Large Datasets, 2023. URL <https://arxiv.org/abs/2311.15127>.
- Burgoon, J. K., Birk, T., and Pfau, M. Nonverbal Behaviors, Persuasion, and Credibility. *Human communication research*, 17(1):140–169, 1990.
- Chan, C., Ginosar, S., Zhou, T., and Efros, A. A. Everybody Dance Now. 2019.
- Chang, H., Zhang, H., Barber, J., Maschinot, A., Lezama, J., Jiang, L., Yang, M.-H., Murphy, K., Freeman, W. T., Rubinstein, M., et al. Muse: Text-to-Image Generation Via Masked Generative Transformers. *arXiv preprint arXiv:2301.00704*, 2023.
- Chen, J., Liu, Y., Wang, J., Zeng, A., Li, Y., and Chen, Q. DiffSHEG: A Diffusion-Based Approach for Real-Time Speech-driven Holistic 3D Expression and Gesture Generation, 2024. URL <https://arxiv.org/abs/2401.04747>.
- Chen, S., Wang, C., Chen, Z., Wu, Y., Liu, S., Chen, Z., Li, J., Kanda, N., Yoshioka, T., Xiao, X., et al. WavLM: Large-Scale Self-Supervised Pre-Training for Full Stack Speech Processing. *IEEE Journal of Selected Topics in Signal Processing*, 16(6):1505–1518, 2022.
- De Ruiter, J. P., Bangerter, A., and Dings, P. The Interplay Between Gesture and Speech in the Production of Referring Expressions: Investigating the Tradeoff Hypothesis. *Topics in cognitive science*, 4(2):232–248, 2012.
- Deichler, A., Mehta, S., Alexanderson, S., and Beskow, J. Diffusion-based co-speech gesture generation using joint text and audio representation. In *INTERNATIONAL CONFERENCE ON MULTIMODAL INTERACTION, ICMI '23*. ACM, October 2023. doi: 10.1145/3577190.3616117. URL <http://dx.doi.org/10.1145/3577190.3616117>.
- Devlin, J. BERT: Pre-Training of Deep Bidirectional Transformers for Language Understanding. *arXiv preprint arXiv:1810.04805*, 2018.
- Ginosar, S., Bar, A., Kohavi, G., Chan, C., Owens, A., and Malik, J. Learning Individual Styles of Conversational Gesture. IEEE, June 2019.
- Guo, C., Mu, Y., Javed, M. G., Wang, S., and Cheng, L. Momask: Generative masked modeling of 3d human motions. In *Proceedings of the IEEE/CVF Conference on Computer Vision and Pattern Recognition*, pp. 1900–1910, 2024a.
- Guo, Y., Yang, C., Rao, A., Liang, Z., Wang, Y., Qiao, Y., Agrawala, M., Lin, D., and Dai, B. AnimateDiff: Animate Your Personalized Text-to-Image Diffusion Models without Specific Tuning. 2024b.
- He, K., Chen, X., Xie, S., Li, Y., Dollár, P., and Girshick, R. Masked Autoencoders Are Scalable Vision Learners. pp. 16000–16009, 2022.
- He, X., Wandt, B., and Rhodin, H. AutoLink: Self-Supervised Learning of Human Skeletons and Object Outlines by Linking Keypoints, 2023. URL <https://arxiv.org/abs/2205.10636>.
- He, X., Huang, Q., Zhang, Z., Lin, Z., Wu, Z., Yang, S., Li, M., Chen, Z., Xu, S., and Wu, X. Co-Speech Gesture Video Generation via Motion-Decoupled Diffusion Model. pp. 2263–2273, 2024.
- Hu, E. J., Shen, Y., Wallis, P., Allen-Zhu, Z., Li, Y., Wang, S., Wang, L., and Chen, W. LoRA: Low-Rank Adaptation of Large Language Models. 2022. URL <https://openreview.net/forum?id=nZeVKeeFYf9>.

- Hu, L., Gao, X., Zhang, P., Sun, K., Zhang, B., and Bo, L. Animate Anyone: Consistent and Controllable Image-to-Video Synthesis for Character Animation. *arXiv preprint arXiv:2311.17117*, 2023.
- Huang, X. and Belongie, S. Arbitrary Style Transfer in Real-time with Adaptive Instance Normalization, 2017. URL <https://arxiv.org/abs/1703.06868>.
- Huang, Z., Tang, F., Zhang, Y., Cun, X., Cao, J., Li, J., and Lee, T.-Y. Make-your-anchor: A diffusion-based 2d avatar generation framework. *arXiv preprint arXiv:2403.16510*, 2024.
- Jiang, T., Lu, P., Zhang, L., Ma, N., Han, R., Lyu, C., Li, Y., and Chen, K. RtmPose: Real-time multi-person pose estimation based on mmpose, 2023. URL <https://arxiv.org/abs/2303.07399>.
- Johnson, J., Alahi, A., and Fei-Fei, L. Perceptual Losses for Real-Time Style Transfer and Super-Resolution, 2016. URL <https://arxiv.org/abs/1603.08155>.
- Karras, J., Holynski, A., Wang, T.-C., and Kermeler-Shlizerman, I. DreamPose: Fashion Image-to-Video Synthesis via Stable Diffusion. *arXiv preprint arXiv:2304.06025*, 2023.
- Kingma, D. P. Adam: A Method for Stochastic Optimization. *arXiv preprint arXiv:1412.6980*, 2014.
- Lee, D., Kim, C., Kim, S., Cho, M., and Han, W.-S. Autoregressive Image Generation Using Residual Quantization, 2022. URL <https://arxiv.org/abs/2203.01941>.
- Lee, H.-Y., Yang, X., Liu, M.-Y., Wang, T.-C., Lu, Y.-D., Yang, M.-H., and Kautz, J. Dancing to Music. 32, 2019.
- Li, R., Yang, S., Ross, D. A., and Kanazawa, A. AI Choreographer: Music Conditioned 3D Dance Generation with AIST++. In *Proceedings of the IEEE/CVF International Conference on Computer Vision*, pp. 13401–13412, 2021.
- Li, T., Chang, H., Mishra, S., Zhang, H., Katabi, D., and Krishnan, D. MAGE: Masked Generative Encoder to Unify Representation Learning and Image Synthesis. pp. 2142–2152, 2023.
- Liu, H., Iwamoto, N., Zhu, Z., Li, Z., Zhou, Y., Bozkurt, E., and Zheng, B. DisCo: Disentangled Implicit Content and Rhythm Learning for Diverse Co-Speech Gestures Synthesis. In *Proceedings of the 30th ACM International Conference on Multimedia*, pp. 3764–3773, 2022a.
- Liu, H., Zhu, Z., Iwamoto, N., Peng, Y., Li, Z., Zhou, Y., Bozkurt, E., and Zheng, B. BEAT: A Large-Scale Semantic and Emotional Multi-Modal Dataset for Conversational Gestures Synthesis. *arXiv preprint arXiv:2203.05297*, 2022b.
- Liu, H., Zhu, Z., Becherini, G., Peng, Y., Su, M., Zhou, Y., Iwamoto, N., Zheng, B., and Black, M. J. EMAGE: Towards Unified Holistic Co-Speech Gesture Generation via Masked Audio Gesture Modeling. *arXiv preprint arXiv:2401.00374*, 2023.
- Liu, X., Wu, Q., Zhou, H., Du, Y., Wu, W., Lin, D., and Liu, Z. Audio-Driven Co-Speech Gesture Video Generation. 35:21386–21399, 2022c.
- Liu, X., Wu, Q., Zhou, H., Xu, Y., Qian, R., Lin, X., Zhou, X., Wu, W., Dai, B., and Zhou, B. Learning Hierarchical Cross-Modal Association for Co-Speech Gesture Generation. pp. 10462–10472, 2022d.
- Liu, Y., Ott, M., Goyal, N., Du, J., Joshi, M., Chen, D., Levy, O., Lewis, M., Zettlemoyer, L., and Stoyanov, V. Roberta: A robustly optimized bert pretraining approach, 2019. URL <https://arxiv.org/abs/1907.11692>.
- Mao, X., Jiang, Z., Wang, Q., Fu, C., Zhang, J., Wu, J., Wang, Y., Wang, C., Li, W., and Chi, M. Mdt-a2g: Exploring masked diffusion transformers for co-speech gesture generation. In *Proceedings of the 32nd ACM International Conference on Multimedia*, MM '24, pp. 3266–3274. ACM, October 2024. doi: 10.1145/3664647.3680684. URL <http://dx.doi.org/10.1145/3664647.3680684>.
- McFee, B., Raffel, C., Liang, D., Ellis, D. P., McVicar, M., Battenberg, E., and Nieto, O. librosa: Audio and Music Signal Analysis in Python. In *Proceedings of the 14th Python in Science Conference*, volume 8, 2015.
- Meng, R., Zhang, X., Li, Y., and Ma, C. Echomimicv2: Towards striking, simplified, and semi-body human animation, 2024.
- OpenMMLab. OpenMMLab Pose Estimation Toolbox and Benchmark. <https://github.com/open-mmlab/mmpose>, 2020.
- Park, T., Liu, M.-Y., Wang, T.-C., and Zhu, J.-Y. Semantic Image Synthesis with Spatially-Adaptive Normalization. 2019.
- Pavlakos, G., Choutas, V., Ghorbani, N., Bolkart, T., Osman, A. A. A., Tzionas, D., and Black, M. J. Expressive Body Capture: 3D Hands, Face, and Body from a Single Image. 2019.
- Petrovich, M., Black, M. J., and Varol, G. Tmr: Text-to-motion retrieval using contrastive 3d human motion synthesis, 2023. URL <https://arxiv.org/abs/2305.00976>.

- Pinyoanuntapong, E., Wang, P., Lee, M., and Chen, C. MMM: Generative Masked Motion Model. pp. 1546–1555, 2024.
- Rabiner, L. and Schafer, R. *Theory and Applications of Digital Speech Processing*. Prentice Hall Press, 2010.
- Ruan, L., Ma, Y., Yang, H., He, H., Liu, B., Fu, J., Yuan, N. J., Jin, Q., and Guo, B. MM-Diffusion: Learning Multi-Modal Diffusion Models for Joint Audio and Video Generation. 2023.
- Selvadurai, A. and Selvadurai, A. The Biharmonic Equation. *Partial Differential Equations in Mechanics 2: The Biharmonic Equation, Poisson’s Equation*, pp. 1–502, 2000.
- Siarohin, A., Lathuilière, S., Tulyakov, S., Ricci, E., and Sebe, N. First Order Motion Model for Image Animation. 2019.
- Siarohin, A., Woodford, O., Ren, J., Chai, M., and Tulyakov, S. Motion Representations for Articulated Animation. 2021.
- Siyao, L., Yu, W., Gu, T., Lin, C., Wang, Q., Qian, C., Loy, C. C., and Liu, Z. Bailando: 3D Dance Generation by Actor-Critic GPT with Choreographic Memory. pp. 11050–11059, 2022.
- Tevet, G., Raab, S., Gordon, B., Shafir, Y., Cohen-Or, D., and Bermano, A. H. Human Motion Diffusion Model. *arXiv preprint arXiv:2209.14916*, 2022.
- Tian, L., Wang, Q., Zhang, B., and Bo, L. EMO: Emote Portrait Alive-Generating Expressive Portrait Videos with Audio2Video Diffusion Model Under Weak Conditions. *arXiv preprint arXiv:2402.17485*, 2024.
- Unterthiner, T., Van Steenkiste, S., Kurach, K., Marinier, R., Michalski, M., and Gelly, S. Towards Accurate Generative Models of Video: A New Metric & Challenges. *arXiv preprint arXiv:1812.01717*, 2018.
- van den Oord, A., Vinyals, O., and Kavukcuoglu, K. Neural Discrete Representation Learning, 2018. URL <https://arxiv.org/abs/1711.00937>.
- van den Oord, A., Li, Y., and Vinyals, O. Representation learning with contrastive predictive coding, 2019. URL <https://arxiv.org/abs/1807.03748>.
- Wan, Q., Zhang, W., and Xue, X. DeepSkeleton: Skeleton Map for 3D Human Pose Regression, 2017. URL <https://arxiv.org/abs/1711.10796>.
- Wang, C. T2m-hifigt: Generating high quality human motion from textual descriptions with residual discrete representations, 2023. URL <https://arxiv.org/abs/2312.10628>.
- Wang, T., Li, L., Lin, K., Lin, C.-C., Yang, Z., Zhang, H., Liu, Z., and Wang, L. DisCo: Disentangled Control for Referring Human Dance Generation in Real World. *arXiv preprint arXiv:2307.00040*, 2023.
- Wang, T.-C., Liu, M.-Y., Zhu, J.-Y., Tao, A., Kautz, J., and Catanzaro, B. High-Resolution Image Synthesis and Semantic Manipulation with Conditional GANs. In *CVPR*, 2018.
- Wu, H., Zhang, E., Liao, L., Chen, C., Hou, J. H., Wang, A., Sun, W. S., Yan, Q., and Lin, W. Exploring Video Quality Assessment on User Generated Contents from Aesthetic and Technical Perspectives. 2023.
- Xing, J., Xia, M., Zhang, Y., Cun, X., Wang, J., and Wong, T.-T. Codetalker: Speech-driven 3d facial animation with discrete motion prior. In *Proceedings of the IEEE/CVF Conference on Computer Vision and Pattern Recognition*, pp. 12780–12790, 2023.
- Xu, Z., Zhang, Y., Yang, S., Li, R., and Li, X. Chain of generation: Multi-modal gesture synthesis via cascaded conditional control, 2023. URL <https://arxiv.org/abs/2312.15900>.
- Yi, H., Liang, H., Liu, Y., Cao, Q., Wen, Y., Bolkart, T., Tao, D., and Black, M. J. Generating Holistic 3D Human Motion from Speech. 2023.
- Yoon, Y., Cha, B., Lee, J.-H., Jang, M., Lee, J., Kim, J., and Lee, G. Speech Gesture Generation from the Trimodal Context of Text, Audio, and Speaker Identity. *ACM Transactions on Graphics*, 39(6), 2020.
- Zhao, J. and Zhang, H. Thin-Plate Spline Motion Model for Image Animation. pp. 3657–3666, 2022.
- Zhu, S., Chen, J. L., Dai, Z., Xu, Y., Cao, X., Yao, Y., Zhu, H., and Zhu, S. Champ: Controllable and Consistent Human Image Animation with 3D Parametric Guidance. *arXiv preprint arXiv:2403.14781*, 2024.

Contextual Gesture: Co-Speech Gesture Video Generation Through Context-Aware Gesture Representation

Supplementary Material

A. Overview

The supplementary material is organized into the following sections:

- Section B: Additional Related Works
- Section C: Dataset Details and Preprocessing
- Section D: Additional Implementation Details
- Section E: Gesture Motion Generation
- Section F: Gesture Speech Retrieval
- Section G: Additional Experiments
- Section H: Time and Resource Consumption
- Section I: User Study Details
- Section J TPS-based Image Warping
- Section K Ethical Ethical Considerations
- Section L: Limitations

For more visualization, please see the additional demo videos.

B. Additional Related Works

Masked Representation Learning for Generation Masked Representation Learning has been demonstrated an effective representation learning for various modalities. (Devlin, 2018; He et al., 2022) Some works explored the generation capabilities using this paradigm. MAGE (Li et al., 2023) achieves high-quality image generation through iterative remasking. Muse (Chang et al., 2023) extends this idea to leverage language with region masking for image editing and achieve fine-grained control. Recent Masking Models (Pinyoanuntapong et al., 2024; Guo et al., 2024a; Wang, 2023; Mao et al., 2024) bring this strategy to the motion and gesture domain and improves the motion generation speed, quality, and editing capability. Inspired by these work, we propose the masked gesture generation conditioned the audio to learn the gesture-speech correspondence during generation.

C. Dataset Details and Preprocessing

C.1. Preprocessing

We found that many videos used in ANGIE (Liu et al., 2022c) and S2G-Diffusion (He et al., 2024), particularly for the subject *Jon*, are no longer available. To address this, we replaced *Jon* with *Noah*. We utilized the PATS (Ginosar et al., 2019) metadata to download videos from YouTube and preprocess them. After filtering, we obtained 1080 videos for *Oliver*, 1080 for *Kubinec*, 1080 for *Seth*, and 988 for *Noah*. For the testing dataset, we collected 120 videos for *Oliver*, 120 for *Kubinec*, 120 for *Seth*, and 94 for *Noah*.

During the dataset preprocessing, while for image-generation we use the whole video preprocessed as above, for for the speech-gesture alignment and gesture pattern generation modules, we further preprocess the data by slicing them into smaller chunks following S2G-Diffusion (He et al., 2024). Specifically, based on the source training dataset, the keypoint sequences and audio sequences are clipped to 80 frames (3.2s) with stride 10 (0.4s) for training. We obtain 85971 overlapping training examples and 8867 testing examples for gesture pattern modeling.

C.2. Feature Representation

Gesture Keypoints. We utilize RTMPose (Jiang et al., 2023) from MMPose (OpenMMLab, 2020) for whole-human-body keypoint identification. The keypoint definition is based on by 133 CoCo human pose estimation. Due to the PATS (Ginosar et al., 2019) only contains the upper body, we select 68 face landmarks for face motion modeling, 3 for left shoulder, 3 for right shoulder, 21 for left hand and 21 for right hand separately, which results in flattened face feature with dim of 136 and body feature with dim of 96.

Audio Features. The audio features are pre-extracted WavLM features (dim of 1024) with additional low-level mel-spectrum and beat information with dimension of 34. We concatenate them channel-wise as the speech feature.

C.3. Dataset License.

The video data within PATS dataset include personal identity information, and we strictly adhere to the data usage license “CC BY - NC - ND 4.0 International,” which permits non-commercial use.

D. Additional Implementation Details

We jointly train the framework on three speakers. The following sections provide the details for each module’s training.

Optimizer Settings. All modules utilize the Adam Optimizer (Kingma, 2014) during training, with a learning rate of 1×10^{-4} , $\beta_1 = 0.5$, and $\beta_2 = 0.999$.

Speech-Gesture Alignment. For aligning speech with facial and bodily gestures, we implement two standard transformer blocks for encoding each modality. The latent dimension is configured to 384, accompanied by a feedforward size of 1024. We calculate the mean features for both modalities and project them using a two-layer MLP in a contrastive learning framework, with a temperature parameter set to 0.7.

Residual Vector Quantization (RVQ) Tokenization. The overall training objective for the RVQ-VAE is defined as:

$$\mathcal{L}_{\text{rvq}} = \mathbb{E}_{x \sim p(x)} \left[\|x - \hat{x}\|^2 \right] + \alpha \sum_{r=1}^R \mathbb{E}_{z_r \sim q(z_r|x)} \left[\|e_r - \text{sg}(z_r - e_r)\|^2 \right] + \beta \mathcal{L}_{\text{distill}} \quad (9)$$

where \mathcal{L}_{rvq} combines a motion reconstruction loss, a commitment loss (van den Oord et al., 2018) for each layer of quantizer with a distillation loss, with α and β weighting the contributions.

We employ six layers of codebooks for residual vector quantization (Lee et al., 2022) for both face and body modalities, each comprising 1024 codes. To address potential collapse issues during training, we implement codebook resets. The RVQ encoder and decoder are built with two layers of convolutional blocks and a latent dimension of 128. We avoid temporal down-sampling to ensure the latent features maintain the same temporal length as the original input sequences. During RVQ training, we set $\alpha = 1$ and $\beta = 0.5$ to balance gesture reconstruction with speech-context distillation.

Mask Gesture Generator. The generator takes sequences of discrete tokens for both face and body, derived from the RVQ codebook. This module includes two layers of audio encoders for face and body, initialized based on the Speech-Gesture Alignment. The latent dimension is again set to 384, with a feedforward dimension of 1024, and it features eight layers for both modalities. A two-layer MLP is utilized to project the latent space to the codebook dimension, and cross-entropy is employed for model training. We calculate reconstruction and acceleration loss by feeding the predicted tokens into the RVQ decoder. A reconstruction loss of 50 is maintained during training, and the mask ratio is uniformly varied between 0.5 and 1.0. For inference, a cosine schedule is adopted for decoding. We uniformly mask between 50% and 100% of the tokens during training. Following the BERT (Devlin, 2018), when a token is selected for masking, we replace it with a [MASK] token 80% of the time, a random token 10% of the time, and leave it unchanged 10% of the time. The Mask Gesture Generator is trained over 250 epochs, taking approximately 1 days to complete.

Residual Gesture Generator. The Residual Gesture Generator is designed similarly to the Mask Gesture Generator but utilizes only six layers for the generator. It features four embedding and classification layers corresponding to the RVQ

Table 3: Ablations of our method. We exam training & inference strategy. Bold indicates the best performance.

<i>M-Ratio</i>	FGD↓	Div.↑	PCM↑		<i>iter.</i>	FGD↓	Div.↑	PCM↑
Uni 0-1	2.13	14.31	0.56		5	0.87	13.23	0.59
Uni .3-1	1.56	12.44	0.512		10	0.98	13.11	0.57
Uni .5-1	0.87	13.23	0.59		15	1.24	13.04	0.57
Uni .7-1	1.22	13.12	0.57		20	1.56	13.23	0.57

(a) mask-ratio during training. (b) Mask decoding steps.

tokenization scheme for residual layers. During training, we randomly select a quantizer layer $j \in [1, R]$ for learning. All tokens from the preceding layers $t^{0:j-1}$ are embedded and summed to form the token embedding input. After generating the base layer predictions of discrete tokens from the Masked Gesture Generator, these tokens are fed into the Residual Gesture Generator. This module iteratively predicts the tokens from the base layers, ultimately producing the final quantized output. This module is trained for an additional 500 epochs, requiring about 0.5 days to finalize.

Image Warping. For pixel-level motion generation, we utilize Thin Plate Splines (TPS) (Zhao & Zhang, 2022). Our framework tracks 116 keypoints (68 for the face and 48 for the body). The number of TPS transformations K is set to 29, with each transformation utilizing $N = 4$ paired keypoints. In accordance with TPS methodologies, both the dense motion network and occlusion-aware generators leverage 2D convolutions to produce 64×64 weight maps for optical flow generation, along with four occlusion masks at various resolutions (32, 64, 128, and 256) to facilitate image frame synthesis.

Structure-aware Image-Refinement. We use the UNet similar to S2G-Diffusion (He et al., 2024) to restore missing details, further improve the hand and shoulder areas. We keep the training loss to be the same except the added conditional adversarial loss based on edge heatmap. For the network design difference, we add the multi-level edge heatmap as additional control for different resolutions (32, 64 and 128). Each corresponds to a SPADE (Park et al., 2019) block to inject the semantic control into the current generation.

E. Gesture Motion Generation

Inference. While existing works (Liu et al., 2023; Yi et al., 2023; Chen et al., 2024) leverage auto-regressive next-token prediction or diffusion-based generation process, these strategies hinder the fast synthesis for real-time applications. To resolve this problem, as in Fig. 3, we employ an iterative mask prediction strategy to decode motion tokens during inference. Initially, all tokens are masked except for the first token from the source frame. Conditioned on the audio input, the Mask Gesture Generator predicts probabilities for the masked tokens. In the l -th iteration, the tokens with the lowest confidence are re-masked, while the remaining tokens stay unchanged for subsequent iterations. This updated sequence continues to inform predictions until the final iteration, when the base-layer tokens are fully generated. Upon completion, the Residual Gesture Generator uses the predicted base-layer tokens to progressively generate sequences for the remaining quantization layers. Finally, all tokens are transformed back into motion sequences via the RVQ-VAE decoder.

Training Objective. To train our gesture generation models, \mathcal{L}_{mask} , and \mathcal{L}_{res} functions for two generators respectively by minimizing the categorical cross-entropy loss, as illustrated below:

$$\mathcal{L}_{mask} = \sum_{i=1}^T -\log p_{\phi}(t_i | Es(S), \text{MASK}), \quad \mathcal{L}_{res} = \sum_{j=1}^V \sum_{i=1}^T -\log p_{\phi}(t_i^j | t_i^{1:j-1}, Es(S), j). \quad (10)$$

In this formulation, \mathcal{L}_{mask} predicts the masked motion tokens t_i at each time step i based on the input audio and the special [MASK] token. Conversely, \mathcal{L}_{res} focuses on learning from multiple quantization layers, where t_i^j represents the motion token from quantizer layer j and $t_i^{1:j-1}$ includes the tokens from preceding layers. We also feed the predicted tokens into the RVQ decoder for gesture reconstructions, with velocity and acceleration losses (Tevet et al., 2022; Siyao et al., 2022).

Ablation. We evaluate the mask ratio during training and the number of inference steps during decoding. As shown in Tab. 3b, our model requires only 5 inference steps, in contrast to over 50 or 100 steps in diffusion-based models. Furthermore, a uniform masking ratio between 0.5 and 1 during training yields optimal performance.

Table 4: **Speech-to-Gesture Motion retrieval benchmark on PATS:** We establish two evaluation settings as described in Section F.

Setting	Speech-Face retrieval					Face-Speech retrieval				
	R@1 ↑	R@2 ↑	R@3 ↑	R@5 ↑	R@10 ↑	R@1 ↑	R@2 ↑	R@3 ↑	R@5 ↑	R@10 ↑
(a) All	0.181	0.350	0.485	0.722	1.343	0.226	0.361	0.429	0.677	1.207
(a) + chrono	0.231	0.372	0.501	0.734	1.696	0.323	0.398	0.454	0.712	1.332
(b) Small batches	26.230	45.318	59.330	77.019	89.858	24.977	44.822	59.894	77.775	90.264
(b) + chrono	27.437	47.552	63.193	74.343	89.996	26.451	46.432	61.727	79.779	91.373

Setting	Speech-Body retrieval					Body-Speech retrieval				
	R@1 ↑	R@2 ↑	R@3 ↑	R@5 ↑	R@10 ↑	R@1 ↑	R@2 ↑	R@3 ↑	R@5 ↑	R@10 ↑
(a) All	0.102	0.237	0.327	0.587	1.230	0.158	0.271	0.406	0.654	1.320
(a) + chrono	0.132	0.257	0.373	0.603	1.340	0.178	0.289	0.443	0.671	1.404
(b) Small batches	25.542	43.660	57.954	77.471	90.309	24.052	43.874	58.495	76.986	89.745
(b) + chrono	28.732	48.569	59.958	79.321	90.003	22.671	45.737	57.669	79.565	90.672

F. Speech-Gesture Retrieval

To validate the effectiveness of Speech-Gesture Alignment, inspired by TMR (Petrovich et al., 2023) we propose the Speech-Gesture Retrieval as the evaluation benchmark.

Evaluation Settings. The retrieval performance is measured under recall at various ranks, R@1, R@2, etc. Recall at rank k indicates the percentage of times the correct label is among the top k results; therefore higher is better. We define two settings. The retrieval is based on the sliced clips, with each lasting for 4 seconds and 120 frames, in total 8176 samples.

(a) **All** test set samples for face and body motions. This set is problematic because the speech and gesture motion should not be of one-to-one mapping relationship.

(b) **Small batch** size of 32 speech-gesture pairs are randomly picked, reporting average performance.

Evaluation Result. Shown in Tab. 4, the gesture patterns and speech context do not present one-to-one mapping relationship, leading to the significantly low performance of retrieval. However, based on setting (b), within a small batch size of 32, the model achieves significantly higher performance, indicating the alignment provides the discrimination over different speech context and the motion. In addition, chronological negative examples during contrastive training enhances the robustness of retrieval.

G. Additional Experiments

In the main paper, we have shown our method achieves promising joint gesture motion and video generation. To understand the disentangled gesture and video avatar generation separately, we further conduct Gesture Generation and Video Avatar Animation experiments separately to compare our method with the corresponding representative works for each domain.

G.1. Gesture Generation

Experiment Settings We select BEAT-X (Liu et al., 2023) as the dataset for additional gesture generation comparison. For consistency, we will exclude the image-to-animation component from our method and extend gesture representation from 2D to 3D poses. (with SMPL-X expressions for face gestures, as in the existing literature) We compare the gesture generation module of our work with representative state-of-the-art methods in co-speech gesture generation (Ao et al., 2022; Yi et al., 2023; Liu et al., 2023). We further design a baseline without using contextual distillation.

Evaluation Metrics We evaluate the realism of body gestures by Fréchet Gesture Distance (FGD) (Yoon et al., 2020). We include Diversity by calculating the average L1 distance across generated clips. For synchronization, we use Beat

Table 5: Quantitative results on BEAT-X. FGD (Frechet Gesture Distance) multiplied by 10^{-1} , BC (Beat Constancy) multiplied by 10^{-1} , Diversity, MSE (Mean Squared Error) multiplied by 10^{-7} . The best results are in bold.

Methods	Venue	FGD ↓	BC →	Diversity ↑	MSE ↓
GT			0.703	11.97	
HA2G (Liu et al., 2022d)	CVPR 2022	12.320	0.677	8.626	-
DisCo (Liu et al., 2022a)	ACMMM 2022	9.417	0.643	9.912	-
CaMN (Liu et al., 2022b)	ECCV 2022	6.644	0.676	10.86	-
DiffSHEG (Chen et al., 2024)	CVPR 2024	7.141	0.743	8.21	9.571
TalkShow (Yi et al., 2023)	CVPR 2023	6.209	0.695	13.47	7.791
Rhythmic Gesticulator (Ao et al., 2022)	SIGGRAPH 2023	6.453	0.665	9.132	
EMAGE (Liu et al., 2023)	CVPR 2024	5.512	0.772	13.06	7.680
Ours (w/o distill)	-	5.079	0.737	13.24	7.742
Ours	-	4.434	0.724	13.76	7.021

Constancy (BC) (Li et al., 2021). For facial expression, we use the vertex Mean Squared Error (MSE) (Xing et al., 2023) to for positional accuracy.

Experiment Results As shown in Tab. 5, our method significantly improve the SMPL-X based co-speech gesture generation with lower FGD and higher diversity. Specifically, Our methods have present smoother gesture motion patterns compared with existing works. It demonstrates the effectiveness of contextual distillation for the motion representation learning in our framework. We defer the video comparisons in the Appendix videos for reference.

Long Sequence generation To understand the capability of our framework for long sequence generation, we conduct an ablation study for both PATS and BEAT-X dataset. For BEAT-X, we cut the testing audios into segments of 256 (about 8.53 seconds) for short sequence evaluation and use raw testing audios for long sequence evaluation in Tab. 5. Shown in Tab. 6, it is interesting for PATS dataset, long-sequence generation as an application in the main paper presents quality lower than normal settings. However, for BEAT-X dataset, the generation quality is not affected much. We attribute this difference caused by the dataset difference. Because PATS dataset consists training video lengths with a average of less than 10 seconds, the model presents less diverse gesture patterns. However, in BEAT-X, most of gesture video sequences are over 30 or 1 minutes, our method further benefits from this long sequence learning process and presents higher qualities.

Table 6: Long Sequence Generation Quality.

Dataset	Setting	FGD	Diversity	BAS
PATS	≤10s	1.303	13.260	0.996
	>10s	2.356	11.956	0.994
BEAT-X	≤10s	4.747	13.14	7.323
	>10s	4.650	13.55	7.370

G.2. Video Avatar Animation

Experiment Settings. We select PATS dataset as in main paper for avatar rendering comparison. We processed the videos into 512x512 for Diffusion-based model AnimateAnyone (Hu et al., 2023). We extract the 2D poses by MMPOse (OpenMMLab, 2020) for pose guidance for the Diffusion Model, and maintain all the training details as in AnimateAnyone for consistency.

Experiment Results. We compare the gesture generation module of our work with representative AnimateAnyone (Hu et al., 2023). As shown in Fig. 8, though AnimateAnyone achieves better video generation quality for hand structure of the speaker centering in the video, it fails to maintain the speaker identity, making the avatar less similar to the source image compared with our method. In addition, due to the entanglement of camera motions and speaker gesture motions within the dataset, AnimateAnyone fails to separate two types of motions from the source training video, thus leading to significant background changes over time and dynamic inconsistency. Unlike completely relying on human skeletons as conditions in AnimateAnyone, our method benefits from Warping-based method, which has the capability of resolving the background motions in addition to the speaker motion. We defer visual comparisons in the Appendix videos.

H. Time and Resource Consumption

In Tab. 7, we present a comparison of training and inference times against existing baseline methods. For audio-gesture generation, our model’s training time is comparable, albeit slightly slower, than that of ANGIE (Liu et al., 2022c) and



Figure 8: **Comparison of Video Avatar Animation** Though presented with worse hand structure reconstruction, we achieve better identity preserving and significantly better background motion.

S2G-Diffusion (He et al., 2024), primarily due to the inclusion of additional modules. However, it is considerably faster than MM-Diffusion (Ruan et al., 2023). Notably, our method excels in inference speed, outperforming all other baselines.

While the training of image-warping and image refinement requires a lot of time, our method leads to a substantial reduction in overall time and resource usage compared to MM-Diffusion and other stable-diffusion-based video generation approaches. Furthermore, the generative masking paradigm we employ significantly cuts down inference times when compared to diffusion-based models like S2G-Diffusion or the autoregressive generations in ANGIE.

We further compared image-warping based method computation requirements with Stable Diffusion-based models like AnimateAnyone (Hu et al., 2023) in Tab. 8.

I. User Study Details

For user study, we recruited 20 participants with good English proficiency. To conduct the user study, we randomly select 80 videos from EchoMimicV2 (Meng et al., 2024), ANGIE (Liu et al., 2022c), S2G-Diffusion (He et al., 2024) and ours. Each user works on 20 videos, with 4 videos from each of the aforementioned methods. The users are not informed of the source of the video for fair evaluations. A visualization of the user study is shown in Fig. 9.

Table 7: **Time consumption comparison** of training (1 NVIDIA A100 GPU) and inference (1 NVIDIA GeForce RTX A6000 GPU).

Name	Training	Training Breakdown	Inference (video of ~10 sec)
ANGIE	~5d	Motion Repr. ~3d + Quantize ~0.2d + Gesture GPT ~1.8d	~30 sec
MM-Diffusion	~14d	Generation ~9d + Super-Resolution ~5d	~600 sec
S2G-Diffusion	~5d	Motion Decouple ~3d + Motion Diffusion ~1.5d + Refine ~0.5d	~35 sec
Ours	~6d	Quantize ~0.2d + Mask-Gen ~1.5d + Res-Gen ~0.5d + Img-warp & Refine ~3.5d	~3 sec

Table 8: **Resource consumption comparison** with Stable-Diffusion-based Image-Animation models (1 NVIDIA A100 GPU), * means our re-implementation on PATS dataset.

Methods	Training↓	Batch Size	Resolution	Memory↓	Training Task	Inference↑
AnimateAnyone*	10 days	4	512	44 GB	Pose-2-Img	-
AnimateAnyone*	5 days	4	512	36GB	Img-2-Vid	15s
Ours	2.5 days	64	256	64 GB	Img-Warp	≤1s
Ours	1 day	64	256	48GB	Img-Refine	≤1s
Ours	3.5 days	32	512	60GB	Img-Warp	≤1s
Ours	1 day	32	512	40GB	Img-Refine	≤1s

J. TPS-based Image-Warping

In this paper, we utilize Thin Plate Splines (TPS) (Zhao & Zhang, 2022) to model deformations based on human poses for image-warping. Here, we provide additional details on this approach.

The TPS transformation accepts N pairs of corresponding keypoints (p_i^D, p_i^S) for $i = 1, 2, \dots, N$ (referred to as control points) from a driving image \mathbf{D} and a source image \mathbf{S} . It outputs a pixel coordinate mapping $\mathcal{T}_{tps}(\cdot)$, which represents the backward optical flow from \mathbf{D} to \mathbf{S} . This transformation is founded on the principle that 2D warping can be effectively modeled through a thin plate deformation mechanism. The TPS transformation seeks to minimize the energy associated with bending this thin plate while ensuring that the deformation aligns accurately with the control points. The mathematical formulation is as follows:

$$\begin{aligned} \min \iint_{\mathbb{R}^2} & \left(\left(\frac{\partial^2 \mathcal{T}_{tps}}{\partial x^2} \right)^2 + 2 \left(\frac{\partial^2 \mathcal{T}_{tps}}{\partial x \partial y} \right)^2 + \left(\frac{\partial^2 \mathcal{T}_{tps}}{\partial y^2} \right)^2 \right) dx dy, \\ \text{s.t. } & \mathcal{T}_{tps}(p_i^D) = p_i^S, \quad i = 1, 2, \dots, N, \end{aligned} \quad (11)$$

where p_i^D and p_i^S denote the i^{th} keypoints in \mathbf{D} and \mathbf{S} respectively. As shown in (Zhao & Zhang, 2022), it can be demonstrated that the TPS interpolating function satisfies Eq. (11):

$$\mathcal{T}_{tps}(p) = A \begin{bmatrix} p \\ 1 \end{bmatrix} + \sum_{i=1}^N w_i U(\|p_i^D - p\|_2), \quad (12)$$

where $p = (x, y)^\top$ represents the coordinates in \mathbf{D} , and p_i^D is the i^{th} keypoint in \mathbf{D} . The function $U(r) = r^2 \log r^2$ serves as a radial basis function. Notably, $U(r)$ is the fundamental solution to the biharmonic equation (Selvadurai & Selvadurai, 2000), defined by:

$$\Delta^2 U = \left(\frac{\partial^2}{\partial x^2} + \frac{\partial^2}{\partial y^2} \right)^2 U \propto \delta_{(0,0)}, \quad (13)$$

where the generalized function $\delta_{(0,0)}$ is characterized as:

$$\delta_{(0,0)} = \begin{cases} \infty, & \text{if } (x, y) = (0, 0) \\ 0, & \text{otherwise} \end{cases}, \quad \text{and } \iint_{\mathbb{R}^2} \delta_{(0,0)}(x, y) dx dy = 1, \quad (14)$$

indicating that $\delta_{(0,0)}$ is zero everywhere except at the origin, where it integrates to one.

Subjective Evaluation of Gesture Videos

Thank you for participating in the subjective evaluation.

Instructions (测试说明):

Please watch each video and rate the videos based on Four evaluation metrics.

1. Realness: How realistic the video looks
2. Diversity: How diverse does the gesture pattern present
3. Synchronization: Are speech and gesture synchronized in this video
4. Overall: Overall quality of the video

Please rate each video on a scale of 1 to 5, where 1 is the lowest and 5 is the highest

Group 1


Reference Video	Realness Quality	Diversity Quality	Synchronization Quality	Overall Quality
	1. Terrible, can't recognized as human gestures 2. Poor, it is not real 3. Fair, hard to judge 4. Good, better, it looks real 5. Excellent, it is what a human would do ○ 1 ○ 2 ○ 3 ○ 4 ○ 5	1. Terrible, it is not diverse at all 2. Poor, it is not diverse 3. Fair, it is hard to judge 4. Good, it various but a little bit limited 5. Excellent, it is what a human would do ○ 1 ○ 2 ○ 3 ○ 4 ○ 5	1. Terrible, it is not synchronized at all 2. Poor, it is not synchronized 3. Fair, it is hard to judge 4. Good, it is synchronized but not perfect 5. Excellent, it is perfectly synchronized ○ 1 ○ 2 ○ 3 ○ 4 ○ 5	1. Terrible, it is not good at all 2. Poor, overall quality is bad 3. Fair, it is hard to judge the overall quality 4. Good, the quality is good 5. Excellent, it is a perfect video example ○ 1 ○ 2 ○ 3 ○ 4 ○ 5

Figure 9: Screenshot of user study website.

We denote the i^{th} keypoint in image \mathbf{X} (either \mathbf{D} or \mathbf{S}) as $p_i^{\mathbf{X}} = (x_i^{\mathbf{X}}, y_i^{\mathbf{X}})^{\top}$, and we define:

$$r_{ij} = \|p_i^{\mathbf{D}} - p_j^{\mathbf{D}}\|, \quad i, j = 1, 2, \dots, N.$$

Next, we construct the following matrices:

$$K = \begin{bmatrix} 0 & U(r_{12}) & \cdots & U(r_{1N}) \\ U(r_{21}) & 0 & \cdots & U(r_{2N}) \\ \vdots & \vdots & \ddots & \vdots \\ U(r_{N1}) & U(r_{N2}) & \cdots & 0 \end{bmatrix}, \quad P = \begin{bmatrix} 1 & x_1^{\mathbf{D}} & y_1^{\mathbf{D}} \\ 1 & x_2^{\mathbf{D}} & y_2^{\mathbf{D}} \\ \vdots & \vdots & \vdots \\ 1 & x_N^{\mathbf{D}} & y_N^{\mathbf{D}} \end{bmatrix},$$

$$L = \begin{bmatrix} K & P \\ P^T & 0 \end{bmatrix}, \quad Y = \begin{bmatrix} x_1^{\mathbf{S}} & x_2^{\mathbf{S}} & \cdots & x_N^{\mathbf{S}} & 0 & 0 & 0 \\ y_1^{\mathbf{S}} & y_2^{\mathbf{S}} & \cdots & y_N^{\mathbf{S}} & 0 & 0 & 0 \end{bmatrix}^{\top}.$$

We can then determine the affine parameters $A \in \mathcal{R}^{2 \times 3}$ and the TPS weights $w_i \in \mathcal{R}^{2 \times 1}$ by solving the following equation:

$$[w_1, w_2, \dots, w_N, A]^{\top} = L^{-1}Y. \quad (15)$$

In Eq. (12), the first term $A \begin{bmatrix} p \\ 1 \end{bmatrix}$ represents an affine transformation that aligns the paired control points $(p_i^{\mathbf{D}}, p_i^{\mathbf{S}})$ in linear space. The second term $\sum_{i=1}^N w_i U(\|p_i^{\mathbf{D}} - p\|_2)$ accounts for nonlinear distortions that enable the thin plate to be elevated or depressed. By combining both linear and nonlinear transformations, the TPS framework facilitates precise deformations, which are essential for accurately capturing motion while preserving critical appearance details within our framework.

K. Ethical Considerations

While this work is centered on generating co-speech gesture videos, it also raises important ethical concerns due to its potential for photo-realistic rendering. This capability could be misused to fabricate videos of public figures making statements or attending events that never took place. Such risks are part of a broader issue within the realm of AI-generated photo-realistic humans, where phenomena like deepfakes and animated representations pose significant ethical challenges.

Although it is difficult to eliminate the potential for misuse entirely, our research offers a valuable technical analysis of gesture video synthesis. This contribution is intended to enhance understanding of the technology’s capabilities and limitations, particularly concerning details such as facial nuances and temporal coherence.

In addition, we emphasize the importance of responsible use. We recommend implementing practices such as watermarking generated videos and utilizing synthetic avatar detection tools for photo-realistic images. These measures are vital in mitigating the risks associated with the misuse of this technology and ensuring ethical standards are upheld.

L. Limitations

While our method have achieved significant improvements over existing baselines, there are still two limitations of the current work.

First, the generation quality still exhibit blurries and flickering issues. The intricate structure of hand hinders the generator in understanding the complex motions. In addition, PATS dataset is sourced from in-the-wild videos of low quality. Most frames extracted from videos demonstrate blurry hands, limiting the network learning. Thus, it is important to collect the high-quality gesture video dataset with clearer hands to further enhance the generation quality.

Second, when modeling the whole upper-body, it is hard to achieve synchronized lip movements aligned with the audio. Even though we explicit separate the face motion and body motion to deal with this problem, there is no regularization on lip movement. We would like to defer this problem to the future works that models disentangled and fine-grained motions for each face and body region.